JOURNAL OF MATERIALS SCIENCE 23 (1988) 1841–1850

Behaviour of the complex dielectric function and energy loss spectrum of copper in the [1 1 0] direction in the energy range $2 < \hbar\omega \leqslant 4$ Rydberg

ABU EL-HASSAN SEOUD
Physics Department, Faculty of Science, Tanta University, Tanta, Egypt

The complex wave vector- and frequency-dependent dielectric function, $\varepsilon(\boldsymbol{q}, \omega) = \varepsilon_1(\boldsymbol{q}, \omega) + \varepsilon_2(\boldsymbol{q}, \omega)$, for copper is calculated using realistic band energies and wave functions. The Bloch states $\psi_{\boldsymbol{bk}}(\boldsymbol{r})$ are obtained from the modified augmented plane wave method (MAPW) with the Chodorow potential. Results are presented for the principal direction of $\boldsymbol{q}$, [1 1 0]. About 70 bands and 60 plane waves at 10 $\boldsymbol{k}$-points in the 1/48th of the Brillouin zone are considered. An additional peak was found at the energy loss spectrum of copper whose centre is situated near 2.1 Rydberg, its centre moves gradually to the high energy side with increasing $|\boldsymbol{q}|$. According to our knowledge, it is the first time this result has been calculated theoretically or even measured experimentally in the [1 1 0] direction for copper.

1. Introduction

The response of electrons to a potential causes readjustment of their distribution and gives rise to the screening of the potential involving the well-known quantity, the dielectric function, $\varepsilon(\boldsymbol{q}, \omega) = \varepsilon_1(\boldsymbol{q}, \omega) + \varepsilon_2(\boldsymbol{q}, \omega)$. This quantity plays an important role in the study of various properties, e.g. transport phenomenon, lattice defects, and optical properties. Consequently, it has been the subject of many investigations.

It is shown [1] that a measurement of the angular distribution of inelastically scattered fast electrons is a direct measurement of the imaginary part of the inverse dielectric function of the solid, Im $[-\varepsilon^{-1}(\boldsymbol{q}, \omega)]$ (known as the energy loss spectrum), at the frequency and momentum of the energy transfer to the electrons in the solid. It is also known [2, 3] that peaks in the energy loss spectrum are generally interpreted as excitations of plasmons. They will occur in that energy region where Im $[\varepsilon(\boldsymbol{q}, \omega)]$, ε_2, is small and Re $[\varepsilon(\boldsymbol{q}, \omega)]$, ε_1, vanishes. The plasma frequency is given by the high frequency zero of ε_1. Because the plasmon energy of the electron gas of the same electron density as that of copper is about 0.8 Ry, the observed energy loss spectrum is not free electron like, but its character is ascribed to the interband transition from the 3d-bands to the empty bands. We have proved in our previous calculations [4] that there are two main broad peaks in the energy loss spectrum at the energy range $0 < \hbar\omega \leqslant 2$ Rydberg (Ry). The energy position of those peaks are given in Table I.

From the results given in Table I we notice that the energy positions of both peaks move gradually to higher energies as $|\boldsymbol{q}|$ increases. The movement of energy loss spectrum peaks is discussed latter.

This work is a continuation of our previous work [4–6], in which we have calculated the complex dielectric function of copper in the three main crystal directions [1 0 0], [1 1 0] and [1 1 1].

2. Method of calculation

The microscopic dielectric function is defined by Adler [7]

$$\varepsilon(\boldsymbol{q} + \boldsymbol{K}, \boldsymbol{q} + \boldsymbol{K}', \omega) = \delta_{\boldsymbol{K},\boldsymbol{K}'} - \frac{4\pi e^2}{\Omega_0(\boldsymbol{q} + \boldsymbol{K})^2} \times \alpha(\boldsymbol{q} + \boldsymbol{K}, \boldsymbol{q} + \boldsymbol{K}', \omega) \quad (1)$$

where the irreducible polarization function $\alpha(\boldsymbol{q} + \boldsymbol{K}, \boldsymbol{q} + \boldsymbol{K}', \omega)$ is given in the random phase approximation by the following sum over occupied and unoccupied Bloch states:

$$\alpha(\boldsymbol{q} + \boldsymbol{K}, \boldsymbol{q} + \boldsymbol{K}', \omega) = 2 \sum_{b,b',\boldsymbol{k}} \langle b\boldsymbol{k} | \exp(-i(\boldsymbol{q} + \boldsymbol{K})\boldsymbol{r}) | b', \boldsymbol{k} + \boldsymbol{q} \rangle \times X \langle b', \boldsymbol{k} + \boldsymbol{q} | \exp[i(\boldsymbol{q} + \boldsymbol{K}')\boldsymbol{r}] | b\boldsymbol{k} \rangle \times X \frac{f(b, \boldsymbol{k}) - f(b', \boldsymbol{k} + \boldsymbol{q})}{E(b, \boldsymbol{k}) - E(b', \boldsymbol{k} + \boldsymbol{q}) + \hbar\omega + i\eta} \quad (2)$$

Ω_0 is the crystal volume, $E(b, \boldsymbol{k})$ is the energy and $\langle \boldsymbol{r} | b\boldsymbol{k} \rangle = \psi_{b\boldsymbol{k}}(\boldsymbol{r})$ is a Bloch state wave function

TABLE I The peaks position for the $\boldsymbol{q}$ vectors in the [1 1 0] direction at the energy range $0 < \hbar\omega \leqslant 2$ Ry [4] in units of $2\pi a^{-1}$, where a is the lattice constant

$\boldsymbol{q}$	1. Peak (Ry)	2. Peak (Ry)
$(\frac{1}{4}, \frac{1}{4}, 0)$	1.45	1.92
$(\frac{1}{2}, \frac{1}{2}, 0)$	1.50	1.93
$(\frac{3}{4}, \frac{3}{4}, 0)$	1.64	1.95
(1, 1, 0)	1.74	1.98

0022–2461/88 $03.00 + .12

characterized by the wave vector $\boldsymbol{k}$ and the band index b, and $f(b, \boldsymbol{k})$ is the occupation number. η is a positive infinitesimally small real number guaranteeing causality. Reciprocal lattice vectors are denoted by $\boldsymbol{K}$ and $\boldsymbol{K}'$. In Appendix 2 the MAPW wave functions are given with the important relations of the MAPW method.

The matrix elements in Equation 2 are integrals over the Winger–Seitz cell.

$$\langle b', \boldsymbol{k} + \boldsymbol{q} | \exp [i(\boldsymbol{q} + \boldsymbol{K})\, \boldsymbol{r}] | b\boldsymbol{k} \rangle = \frac{1}{V_c} \int_{\mathrm{WSC}} \psi^*_{b', \boldsymbol{k}+\boldsymbol{q}}(\boldsymbol{r}) \exp [i(\boldsymbol{q} + \boldsymbol{K})\, \boldsymbol{r}]\, \psi_{b\boldsymbol{k}}(\boldsymbol{r})\, \mathrm{d}^3 r \tag{3}$$

where V_c is the volume of the primitive unit cell. For the calculation of the matrix elements (Equation 3) see Appendix 3. If the vector $(\boldsymbol{k} + \boldsymbol{q})$ lies outside the Brillouin zone it can be brought back into it by the addition of a suitable reciprocal lattice vector $\boldsymbol{Q}^*$.

The appearance of the Fermi–Dirac distribution function in the form $f(b, \boldsymbol{k}) - f(b', \boldsymbol{k} + \boldsymbol{q})$, Equation 2, shows that only the transitions from occupied to non-occupied states make contributions to the dielectric function. The summation over the non-occupied bands is confined in the calculation of the imaginary part, ε_2, over those bands whose energies are lying with a maximum value $\hbar\omega$ over the Fermi energy. On the other hand, the summation in the calculation of the real part, ε_1, is not limited, a point which is missed in the other investigations. For the present purpose, every Bloch function is approximated through about 60 plane waves outside the inscribed APW-sphere and 9 spherical waves inside it. The corresponding eigenvalue problem of the rank 70 means that for every $\boldsymbol{k}$-point there are 70 different eigenstates, 10 below the Fermi level and 60 above it. We have considered the Chodorow potential [8] described in the paper of Burdick [9] throughout the present calculations. To carry out the integrals over the first Brillouin zone (FBZ), the concept of the magic points is used [10, 11], for which 10 $\boldsymbol{k}$-points in the 48th of FBZ are taken into account.

We are interested in the present work in calculation of the diagonal elements of the dielectric matrix in the [1 1 0] direction neglecting the local field effect. We shall discuss the effect of neglecting the non-diagonal elements of the dielectric matrix at the inverse matrix, $\varepsilon^{-1}(\boldsymbol{q}, \omega)$, in Appendix 1.

3. Results

The detailed numerical investigations were done using a $\boldsymbol{k}$-grid with 10 $\boldsymbol{k}$-points in the 1/48th of the Brillouin zone. Due to the desire that the totality of the $\boldsymbol{k}$-points and of the $(\boldsymbol{k} + \boldsymbol{q} + \boldsymbol{Q}^*)$ points coincide, the dielectric function could only be found at the $\boldsymbol{q}$ values (i, j, k) $(2\pi/a)/4$ where i, j and k are integers. We have considered the wave vector $\boldsymbol{q}$ along the [1 1 0] direction.

As a test for the accuracy of our calculations we have studied [4, 5]:

(i) the sum rule, namely,

$$\sum_b |\langle b', \boldsymbol{k} + \boldsymbol{q} + \boldsymbol{Q}^* | \exp [i(\boldsymbol{q}, \boldsymbol{r})]\, | b\boldsymbol{k} \rangle|^2 = 1 \tag{4}$$

for $\boldsymbol{k} = (\frac{1}{4}, \frac{1}{4}, \frac{1}{4})\, 2\pi/a$ and $\boldsymbol{k} = (\frac{1}{8}, \frac{1}{8}, \frac{1}{8})\, 2\pi/a$ as a function of $|\boldsymbol{q}|$. The sum over b in Equation 4 extends over 70 bands from which there are 10 occupied.

(ii) Comparison of our results with the analytical known function (Lindhard function) for a free electron model.

(iii) Qualitative comparison of the static dielectric function (for $\hbar\omega = 10^{-3}$ Ry) with the results of Kubo [12].

(iv) Comparison with the diagonal matrix elements $\varepsilon(\boldsymbol{q} = \boldsymbol{K}, \omega)$ of Mekki [13] calculated with 28 $\boldsymbol{k}$-points in the 48th FBZ.

The accuracy of this test was discussed in detail in our previous work [5]: we refer the reader to that paper. This test shows also that our calculations with 10 $\boldsymbol{k}$ magic points are sufficient for the present purpose. Mekki [14] also calculated $\varepsilon_1(\boldsymbol{q} = 0, \omega)$, $\varepsilon_2(\boldsymbol{q} = 0, \omega)$ and Im $[-1/\varepsilon(\boldsymbol{q} = 0, \omega)]$ with 10 $\boldsymbol{k}$-points by using the MAPW method. His results are in good agreement with the optical measurements of Hagemann *et al.* [15].

The energy loss spectrum of a metal is obtained by:

$$\mathrm{Im}\, [-\varepsilon(\boldsymbol{q}, \omega)^{-1}] = \varepsilon_2(\boldsymbol{q}, \omega)/[\varepsilon_1^2(\boldsymbol{q}, \omega) + \varepsilon_2^2(\boldsymbol{q}, \omega)], \tag{5}$$

if the local field effect is neglected (see Appendix 1).

Our results for Im $[-\varepsilon^{-1}(\boldsymbol{q}, \omega)]$ are given in Fig. 1 for the wave vectors $\boldsymbol{q}$, $(\frac{1}{4}, \frac{1}{4}, 0)$, $(\frac{1}{2}, \frac{1}{2}, 0)$, $(\frac{3}{4}, \frac{3}{4}, 0)$ and (1, 1, 0), in units of $(2\pi/a)$, where a is the lattice constant.

The real and imaginary parts of the complex dielectric function ε_1 and ε_2 are given in Figs 2 to 6. The following notations have been used throughout the work: $\varepsilon_1(\boldsymbol{q}, \omega)$ $(\cdots)$, left ordinate; $\varepsilon_2(\boldsymbol{q}, \omega)$ $(-\cdot-)$, right ordinate. The energy $\hbar\omega$ is given on the abscissa in Rydberg units (1 Ry = 13.6058 eV). The vector $\boldsymbol{P} = \boldsymbol{q} + \boldsymbol{K}$, in units of $2\pi/a$, is given between angled brackets. In this paper $\boldsymbol{K} = (0, 0, 0)$ (i.e. $\boldsymbol{P} = \boldsymbol{q}$).

The values EPSREMAX and EPSREMIN describe the maximum and minimum values of $\varepsilon_1(\boldsymbol{q}, \omega)$, respectively. Similar notations are used for $\varepsilon_2(\boldsymbol{q}, \omega)$, EPSIMMAX and EPSIMMIN. In Figs 3 and 4, $\varepsilon_1(\boldsymbol{q}, \omega)$ and $\varepsilon_2(\boldsymbol{q}, \omega)$ are given separately for $\boldsymbol{q} = (\frac{1}{2}, \frac{1}{2}, 0)\, 2\pi/a$.

4. Discussion

The behaviour of the functions Im $[-\varepsilon^{-1}(\boldsymbol{q}, \omega)]$, $\varepsilon_1(\boldsymbol{q}, \omega)$ and $\varepsilon_2(\boldsymbol{q}, \omega)$ is similar to one another for the first three wave vectors, namely $(\frac{1}{4}, \frac{1}{4}, 0)$, $(\frac{1}{2}, \frac{1}{2}, 0)$ and $(\frac{3}{4}, \frac{3}{4}, 0)$ but for the fourth vector, (1, 1, 0), the position of the peaks and their shapes become different. The same character is noticed in our previous calculations [4] in this direction and in the other two main crystallographic directions [1 0 0] and [1 1 1]. This characteristic behaviour is for all wave vectors such that:

$$|\boldsymbol{q}_\Delta| > |\boldsymbol{q}_\mathrm{X}| \text{ in the } \Delta \text{ direction},$$

$$|\boldsymbol{q}_\Sigma| > |\boldsymbol{q}_\mathrm{K}| \text{ in the } \Sigma \text{ direction},$$

and

$$|\boldsymbol{q}_\Lambda| > |\boldsymbol{q}_\mathrm{L}| \text{ in the } \Lambda \text{ direction},$$

where the high symmetry points X, K and L at the surface of the first Brillouin zone (FBZ) have the

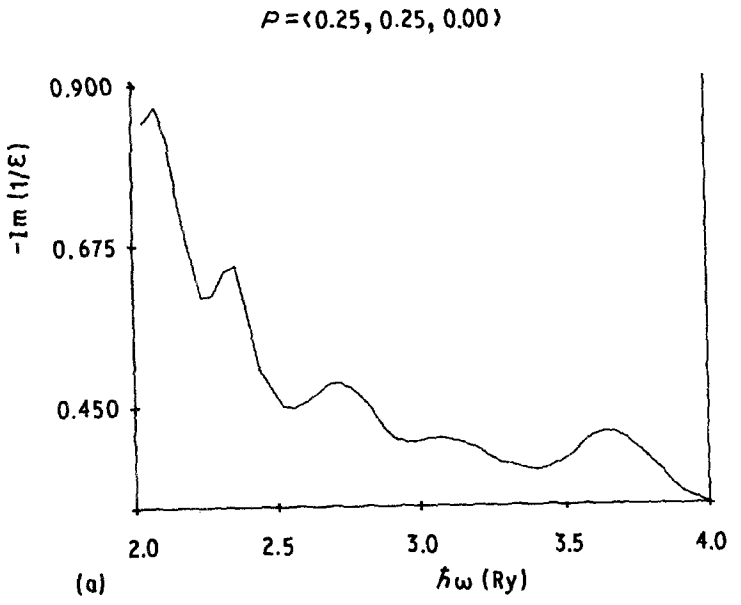

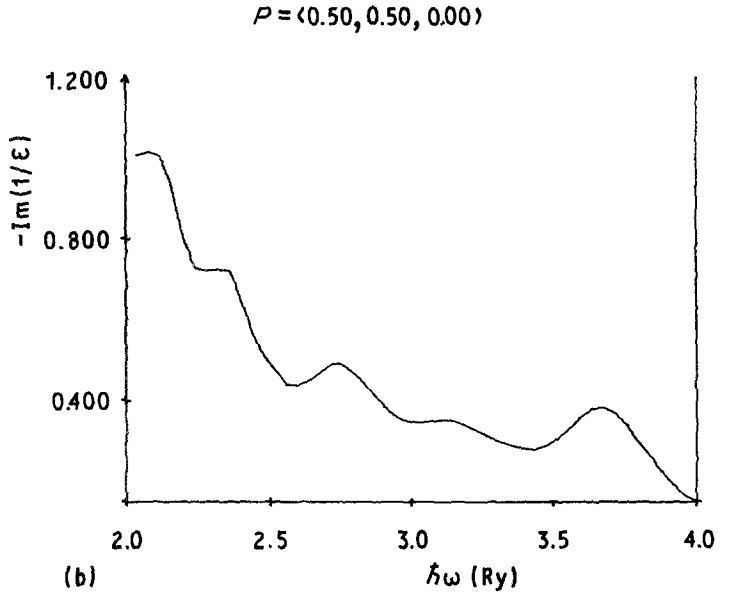

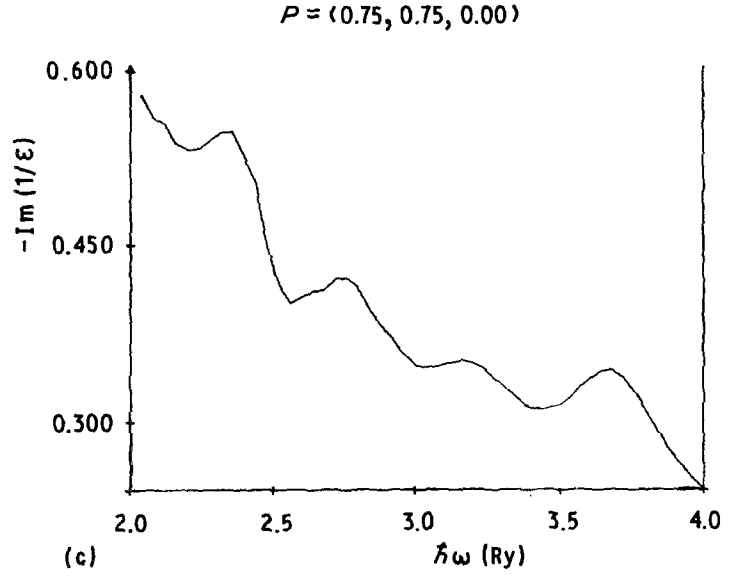

Figure 1 The imaginary part of the inverse dielectric function (the energy loss spectrum $[\mathrm{Im}(-1/\varepsilon)]$) for copper in the [1 1 0] direction: (a) $\boldsymbol{q} = (\frac{1}{4}, \frac{1}{4}, 0)\, 2\pi/a$; (b) $\boldsymbol{q} = (\frac{1}{2}, \frac{1}{2}, 0)\, 2\pi/a$; (c) $\boldsymbol{q} = (\frac{3}{4}, \frac{3}{4}, 0)\, 2\pi/a$; (d) $\boldsymbol{q} = (1, 1, 0)\, 2\pi/a$; in the energy range $2 < \hbar\omega \leqslant 4$ Ry.

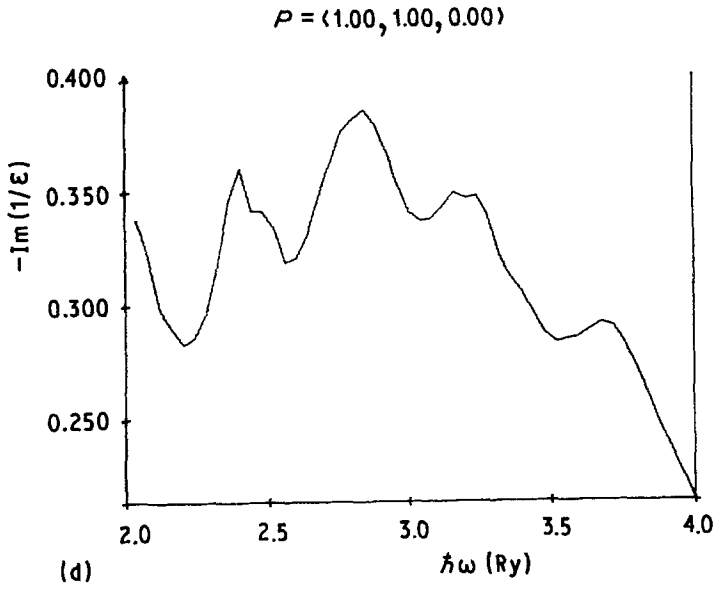

Figure 1 Continued.

coordinates $(2\pi/a)$ (0, 0, 1) $(2\pi/a)$ $(\frac{3}{4}, \frac{3}{4}, 0)$ and $(2\pi/a)$ $(\frac{1}{2}, \frac{1}{2}, \frac{1}{2})$ with respect to the Γ point, respectively. Kubo *et al.* [16] also noticed a characteristic behaviour of the wave vectors $|\boldsymbol{q}| > \frac{3}{4}(2\pi/a)$ from the smaller ones in the [1 0 0] direction.

4.1. Comparison with experiments

If we neglect, for instance, the $\boldsymbol{q}$-dependence of ε for the smallest wave vector [17], namely $\boldsymbol{q}' = (\frac{1}{4}, \frac{1}{4}, 0)$ $2\pi/a$, i.e. $\varepsilon(\boldsymbol{q}', \omega) \approx \varepsilon(\omega)$, then we could be able to use the available experimental results, for example, the optical absorption coefficient, μ, and the density of oscillator strengths $f(E)$. As noted by Wehenkel [18], peaks in $f(E)$ in our energy range occur near minima of Im $(-1/\varepsilon)$. According to the $f(E)$ curve of Feldkamp *et al.* [19], the curve has two minima in our range at 3.09 and 3.67 Ry, which is in a very good agreement with our fourth and fifth peaks (see Fig. 1a). The first peak in our energy loss spectrum (ELS) situated near 2.1 Ry which is very near to the well-known 2.06 Ry peak of Feldkamp *et al.* [19], Wehenkel [18] and Creuzburg [20]. It is also known [21], that peaks in μ are related to a slope change in the ε_2-curve and to a shoulder in the ε_1-curve which appears in the same energy range. According to the μ-curve of Haensel *et al.* (HKS) [22] and that of Wehenkel and Gauthé

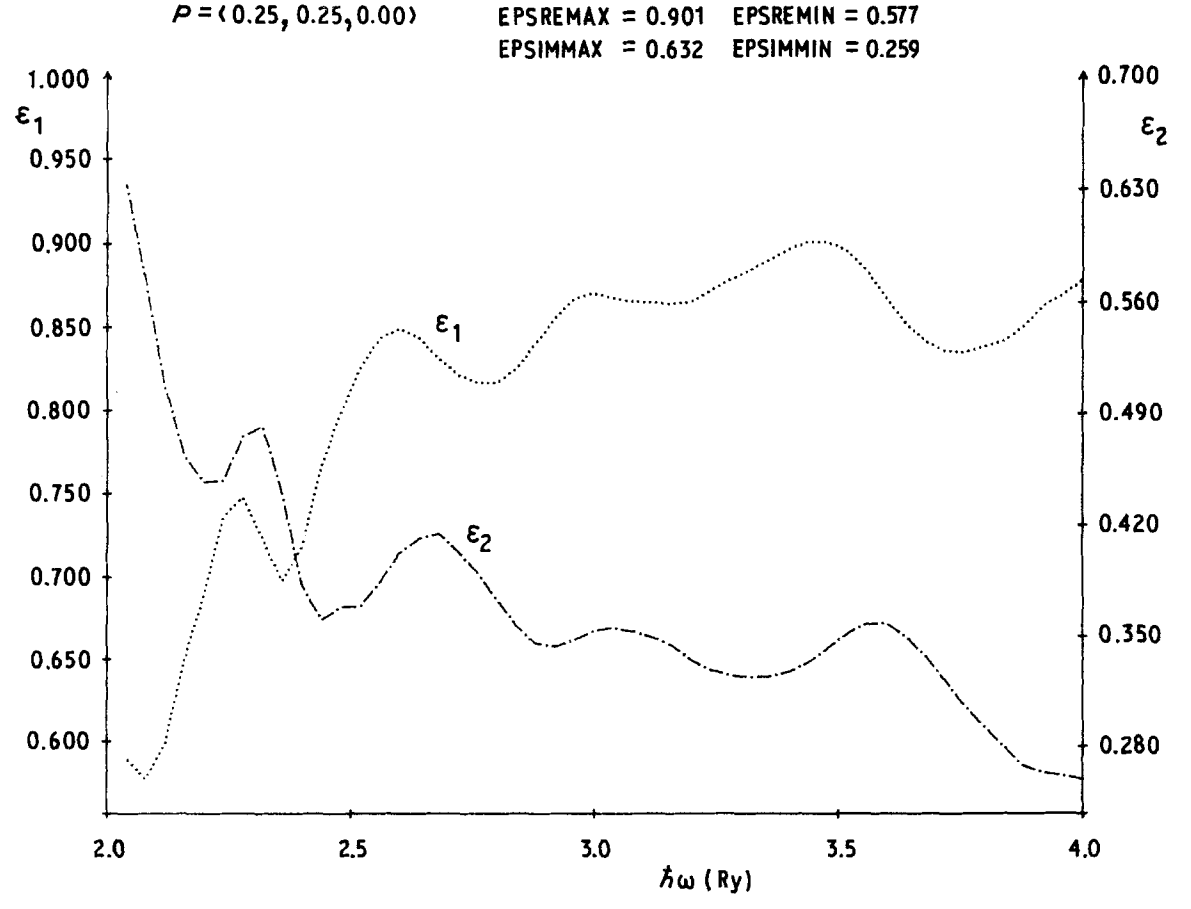

Figure 2 The complex dielectric function for copper, $(\varepsilon = \varepsilon_1 + i\varepsilon_2)$ $\boldsymbol{q} = (\frac{1}{4}, \frac{1}{4}, 0)$ $2\pi/a$, in the energy range $2 < \hbar\omega \leqslant 4$ Ry, $(\cdots)$ ε_1, left ordinate, and $(---)$ ε_2, right ordinate.

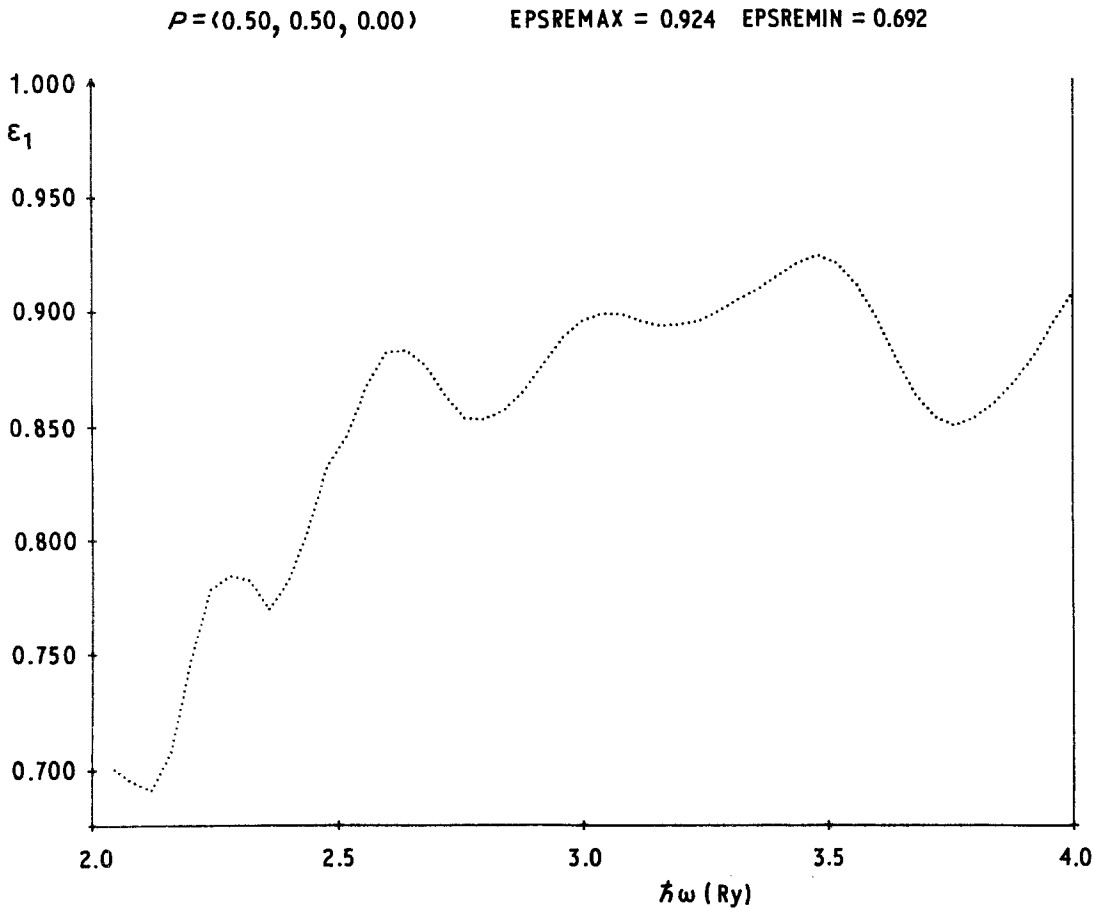

Figure 3 The real part, ε_1, of the copper dielectric function for $\boldsymbol{q} = (\frac{1}{2}, \frac{1}{2}, 0)\ 2\pi/a$ in the energy range $2 < \hbar\omega \leqslant 4$ Ry.

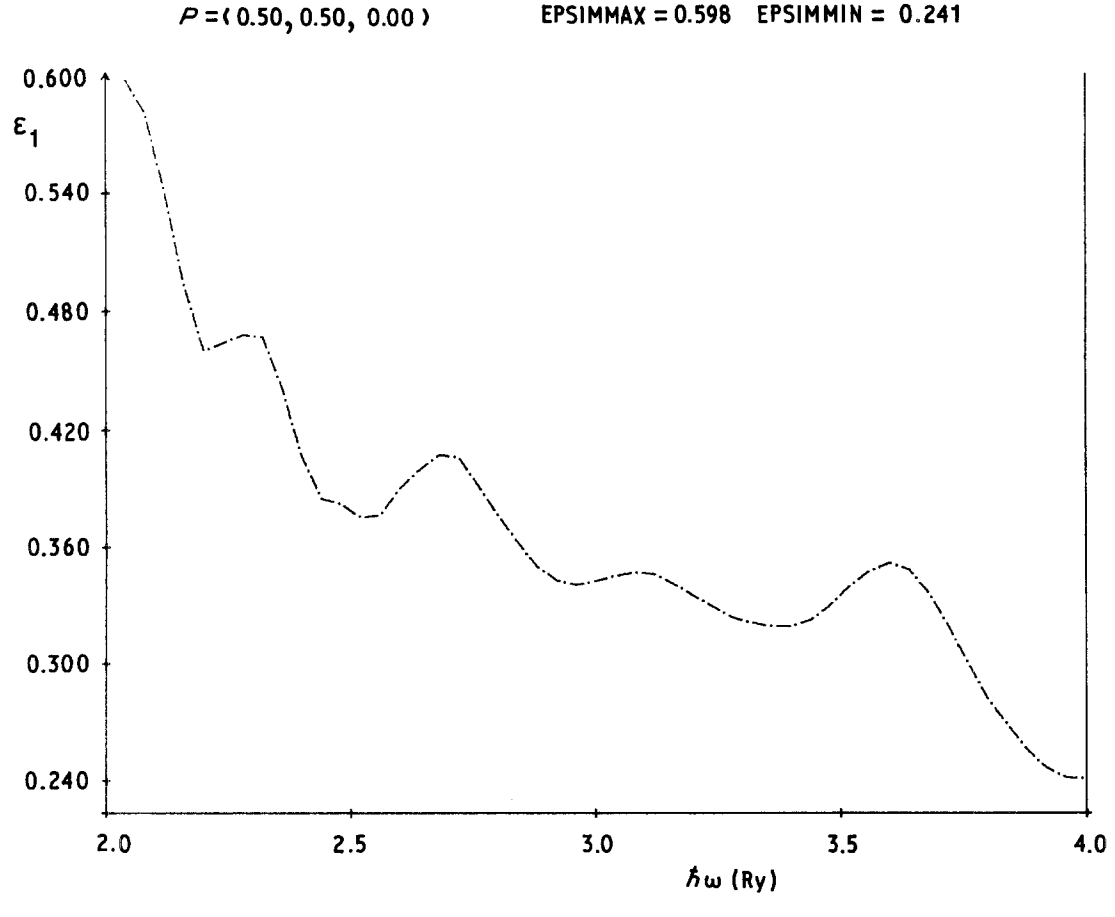

Figure 4 The imaginary part, ε_2, of the copper dielectric function for $\boldsymbol{q} = (\frac{1}{2}, \frac{1}{2}, 0)\ 2\pi/a$ in the energy range $2 < \hbar\omega \leqslant 4$ Ry.

TABLE II The optical absorption coefficient, μ (10^5 cm^{-1}) calculated from Fig. 2 using Equation 6 (as present work) compared with other work

E(Ry)	Present work	HKS[22]	HKSS[24]	SHK[25]	W[18]	WG[23]
2.06	9.8	–	–	–	8.5	8.5
3.10	7.7	7.5	7.6	7.6	5.8	5.8
4.00	7.5	6.7	6.7	6.7	5.2	5.2

(WG) [23], there is a peak at 42 eV (= 3.09 Ry) which is very clear in the HKS-curve and much weaker in the WG-curve. On examining ε_1 and ε_2 curves, Fig. 2, it can be observed that both features are very clear near 3.1 Ry, which indicates that there is a μ-peak around this energy. Moreover, let us calculate the μ-values at some representative energies from Fig. 2 and compare them with those of other workers. The optical absorption coefficient, μ, is given by [21]

$$\mu = \frac{2\omega}{c}\{\tfrac{1}{2}[(\varepsilon_1^2 + \varepsilon_2^2)^{1/2} - \varepsilon_1]\}^{1/2} \qquad (6)$$

Table II shows that our values are in reasonable agreement with those values within experimental error.

4.2. Movement of energy loss spectrum peaks

The movement of ELS peaks to the high energy side with increasing $|\boldsymbol{q}|$ is noticed from Kubo *et al.* [16] in the Δ direction and Seoud [4, 6] in Δ, Σ and Λ directions, which can be explained on the basis of the band structure of copper as a result of electron transitions between broad maxima and minima, as for example near L and Γ points.

4.3. The behaviour of ε_1-curves in the high energy range

It seems for the first time that there is contradiction in our results of the real part $\varepsilon_1[\boldsymbol{q} = (1, 1, 0)\ 2\pi/a, \omega]$ if it is compared with the ε_1-curves for the smaller $\boldsymbol{q}$-vectors, because ε_1 decreases with ω for the first three wave vectors, namely $\boldsymbol{q} = (\frac{1}{4}, \frac{1}{4}, 0)\ 2\pi/a$; $i = 1, 2, 3$, but ε_1 increases with ω (away from the ripples) for $\boldsymbol{q} = (1, 1, 0)\ 2\pi/a$. The reason is that ε_1 at high ω for both copper and from Lindhard [26] are similar. This is reasonable, because in this case we expect copper to resemble a free electron gas because the high energy excited states correspond to loosely bound electrons. This behaviour is also expected because $\varepsilon_1 \approx 1$ for all $\boldsymbol{q}$-vectors considered in this paper, which means that the valence electrons are excited. Let us compare the copper and Lindhard ε_1- curves to prove the similarity between their behaviour in the energy range $2 < \hbar\omega \leqslant 4$ Ry (away from the ε_1^{Cu}-ripples). In Appendix 4 the behaviour of the Lindhard dielectric function is discussed.

For $|\boldsymbol{q}| = 2^{1/2}(2\pi/a)$, i.e. $\boldsymbol{q} = (1, 1, 0)\ 2\pi/a$, ε_1^{Lind} reaches its minimum values, 0.860, at 3.29 Ry then increases to the value 0.933 at 4 Ry [4]. In the case of copper, ε_1^{Cu} has a value of 0.955 at 4 Ry and its value at 3.29 Ry reaches 0.938. For comparison we must study the ε_1^{Lind}-curve for $|\boldsymbol{q}| = 1.0606(2\pi/a)$, i.e. when

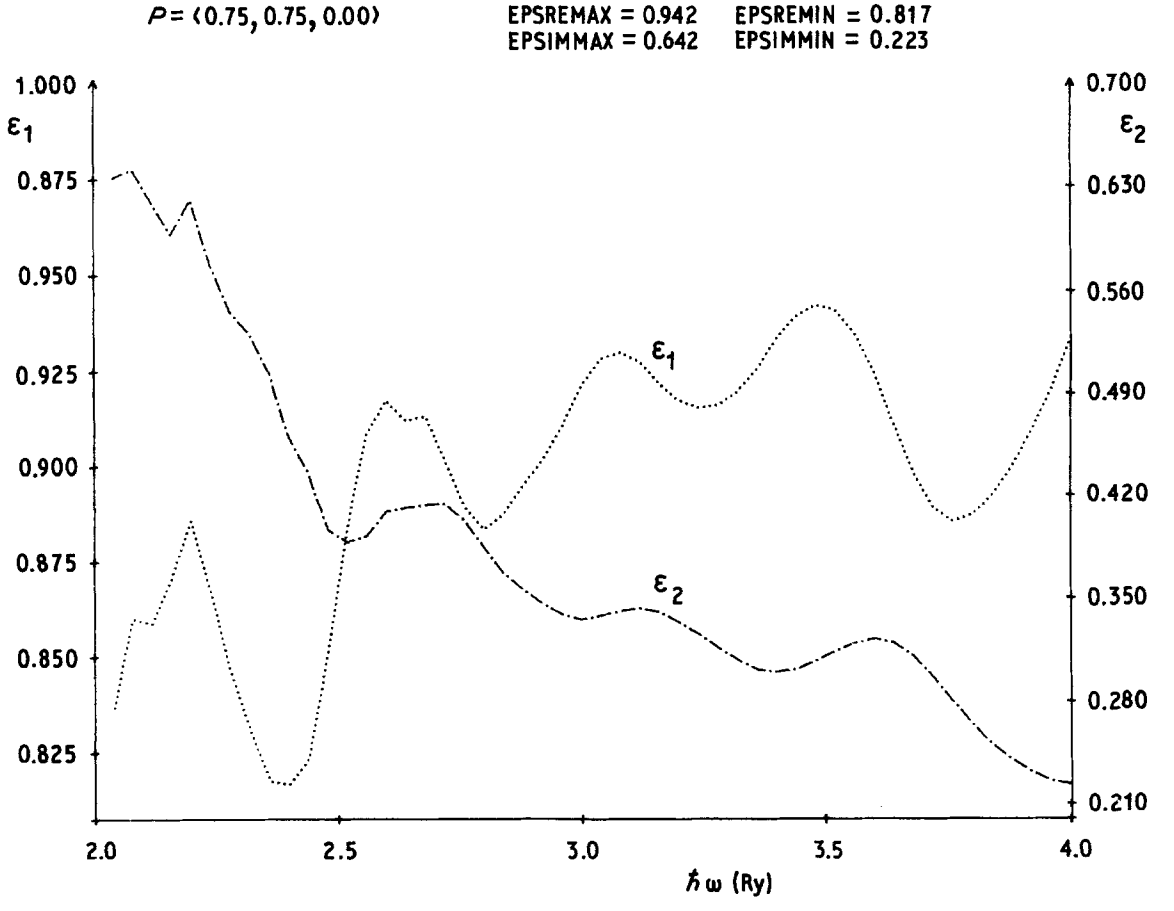

Figure 5 The complex dielectric function for copper, ($\varepsilon = \varepsilon_1 + i\varepsilon_2$) $\boldsymbol{q} = (\frac{3}{4}, \frac{3}{4}, 0)\ 2\pi/a$, in the energy range $2 < \hbar\omega \leqslant 4$ Ry, (···) ε_1, left ordinate, and (– – –) ε_2, right ordinate.

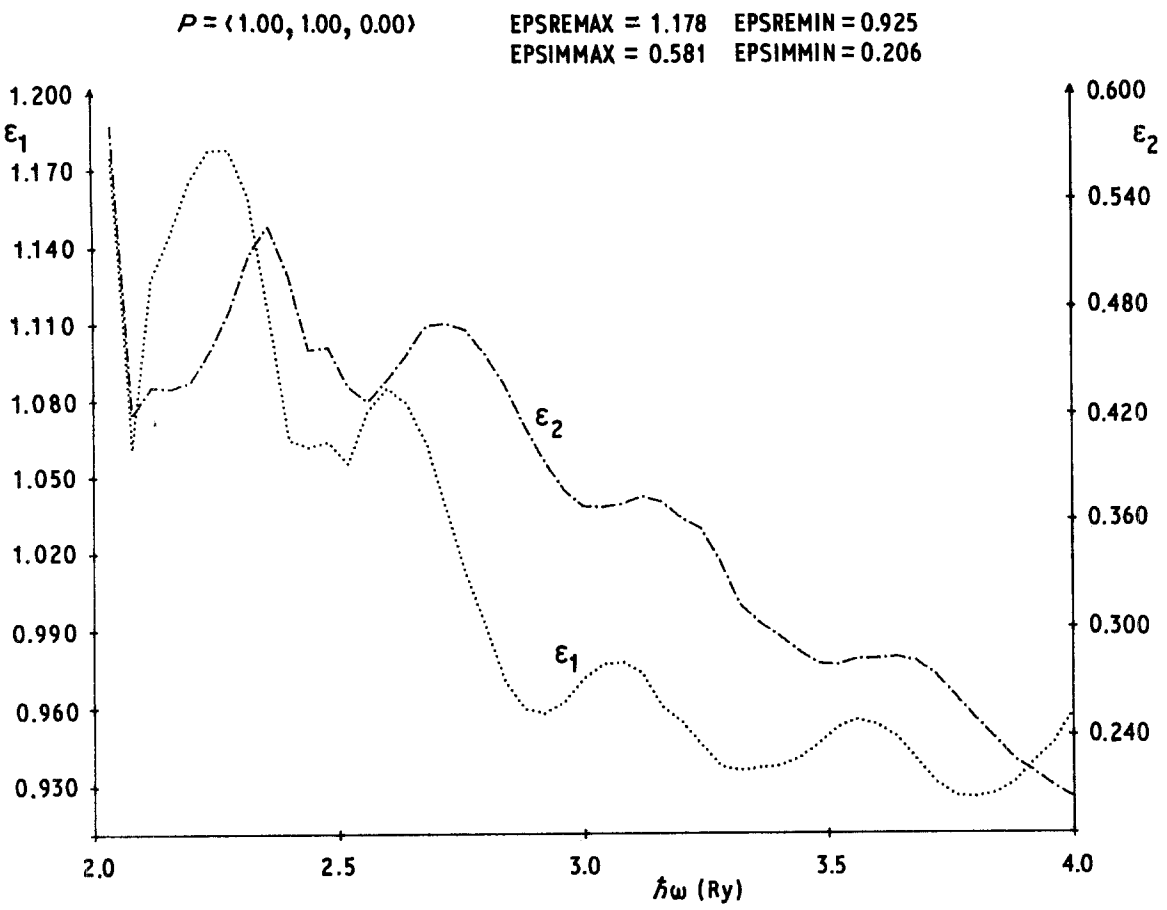

Figure 6 The complex dielectric function for copper ($\varepsilon = \varepsilon_1 + i\varepsilon_2$) $\boldsymbol{q}$ = (1, 1, 0) $2\pi/a$, in the energy range $2 < \hbar\omega \leqslant 4$ Ry, (· · · ·) ε_1, left ordinate, and ε_2, right ordinate.

$\boldsymbol{q} = (\frac{3}{4}, \frac{3}{4}, 0)\ 2\pi/a$ the curve has its minimum value 0.688 at 2.15 Ry then increases with increasing ω and reaches 0.958 at 4 Ry. For copper the ε_1^{Cu} has its minimum 0.817 at 2.37 Ry then increases reaching 0.938 at 4 Ry.

From our previous comparison it is easy to see why ε_1 for $\boldsymbol{q} = (1, 1, 0)\ 2\pi/a$ has a different behaviour from the other smaller wave vectors, but each curve of them has a similar behaviour to the corresponding ε_1^{Lind}-curve.

In Table III, ε_1^{Cu} and ε_1^{Lind} are compared for the same wave vectors at the representative energy $\hbar\omega = 4$ Ry to see that not only do both curves have a similar behaviour but also that the numerical values are very close to each other in our energy range. For more details about the Lindhard function, see Appendix 4.

The origin of the calculated features in ε_2-curves are mainly due to transitions from the 3d occupied bands to the higher empty bands [4, 14, 16, 27]. Also the d–f transition makes a considerable contribution in the high energy range [16].

TABLE III The corresponding numerical values of ε_1^{Lind} [4] and ε_1^{Cu} at $\hbar\omega = 4$ Ry for the given wave vectors in the [1 1 0] direction

$\boldsymbol{q}/\left(\frac{2\pi}{a}\right)$	$\varepsilon_1^{Cu}(\boldsymbol{q}, \hbar\omega = 4\,\text{Ry})$	$\varepsilon_1^{Lind}(\boldsymbol{q}, \hbar\omega = 4\,\text{Ry})$
$(\frac{1}{4}, \frac{1}{4}, 1)$	0.879	0.955
$(\frac{1}{2}, \frac{1}{2}, 0)$	0.994	0.983
$(\frac{3}{4}, \frac{3}{4}, 0)$	0.938	0.958
(1, 1, 0)	0.959	0.933

5. Conclusions

We believe that now is a suitable time for the experimentalists to begin to study and measure the $\boldsymbol{q}$-dependence of the complex dielectric function and energy loss spectrum of real metals, which is of great importance in being able to measure many associated physical phenomena, and for the theoreticians to check their results, which might be useful to correct the calculated band structures of real solids. It is also clear that the calculation of the complex dielectric function and the energy loss spectrum in the high energy range is not of less importance than that of the low energy range, expecially for those metals such as copper, gold and silver, for which plasma frequencies are not defined.

Acknowledgements

The author thanks Professor Dr Bross for the calculation of the band structure of copper used throughout this work. The author is also indebted to Mrs S. Safan for the language correction of the MS.

Appendix 1. The copper local field corrections

The first estimation of the copper non-diagonal elements of the dielectric matrix; those elements with $\boldsymbol{K} \neq \boldsymbol{K}'$ in Equation 1, was first done by Kubo [12], who calculated the static dielectric function of copper, $\varepsilon(\boldsymbol{q}, \omega = 0)$, in the three main principal directions of $\boldsymbol{q}$, [1 0 0], [1 1 0] and [1 1 1]. Kubo considered only the eight nearest neighbour reciprocal lattice vectors during the non-diagonal element calculations, proving

that the non-diagonal elements of the inverse dielectric matrix are fairly small.

Mekki [14] has recently calculated quantitatively, for the first time, the local field effects at the inverse microscopic dielectric matrix $\varepsilon^{-1}(\boldsymbol{q}, \omega)$ in the long wave limit as $\boldsymbol{q} \to 0$ for copper. He considered the contribution from the first and second reciprocal lattice neighbours. Mekki found that the non-diagonal elements of the symmetric hermitian dielectric matrix $x(\boldsymbol{q}, \omega)$ are, in general, smaller by a factor of 7, than the diagonal elements. The elements of x defined as:

$$x(\boldsymbol{q} + \boldsymbol{K}, \boldsymbol{q} + \boldsymbol{K}', \omega) = \delta_{\boldsymbol{K},\boldsymbol{K}'} + 4\pi \frac{\alpha(\boldsymbol{q} + \boldsymbol{K}, \boldsymbol{q} + \boldsymbol{K}', \omega)}{|\boldsymbol{q} + \boldsymbol{K}|\,|\boldsymbol{q} + \boldsymbol{K}'|} \quad \text{(A1)}$$

(see Equation 2) which is connected to the original dielectric matrix elements by

$$\varepsilon(\boldsymbol{q} + \boldsymbol{K}, \boldsymbol{q} + \boldsymbol{K}', \omega) = \frac{|\boldsymbol{q} + \boldsymbol{K}'|}{|\boldsymbol{q} + \boldsymbol{K}|} \times x(\boldsymbol{q} + \boldsymbol{K}, \boldsymbol{q} + \boldsymbol{K}', \omega) \quad \text{(A2)}$$

and its inverse through

$$\varepsilon^{-1}(\boldsymbol{q} + \boldsymbol{K}, \boldsymbol{q} + \boldsymbol{K}', \omega) = \frac{|\boldsymbol{q} + \boldsymbol{K}'|}{|\boldsymbol{q} + \boldsymbol{K}|} \times x^{-1}(\boldsymbol{q} + \boldsymbol{K}, \boldsymbol{q} + \boldsymbol{K}', \omega) \quad \text{(A3)}$$

with:

$$\sum_{\boldsymbol{K}''} x^{-1}(\boldsymbol{q} + \boldsymbol{K}, \boldsymbol{q} + \boldsymbol{K}'', \omega) \times x(\boldsymbol{q} + \boldsymbol{K}'', \boldsymbol{q} + \boldsymbol{K}', \omega) = \delta_{\boldsymbol{K},\boldsymbol{K}'} \quad \text{(A4)}$$

In the previous relations $\varepsilon(\boldsymbol{q} + \boldsymbol{K}, \boldsymbol{q} + \boldsymbol{K}', \omega)$ is a matrix element of the matrix $\boldsymbol{\varepsilon}(\boldsymbol{q}, \omega)$, at which the reciprocal lattice vectors $\boldsymbol{K}$ and $\boldsymbol{K}'$ give numbers to rows and columns, the same notation is used for $x(\boldsymbol{q}, \omega)$ and the inverse matrices.

Mekki [14] also proved that the local field effects in general correct the diagonal elements of $\varepsilon^{-1}(\boldsymbol{K}, \boldsymbol{K}, \omega)$ with a small correction of 5 to 15%.

Appendix 2. MAPW wave functions

The wave functions of the modified augmented plane wave method MAPW [28, 29] are expanded in spherical harmonics and radial solutions of the wave equation within a sphere inscribed in the atomic polyhedron of radius r_0. By suitable choice of the radial functions it is possible to obtain wave-functions which are well orthogonal to the functions of the core electrons. Outside the sphere the wave functions are expanded in plane waves, having the correct translational symmetry, also the wave functions and their first derivatives are continuous in the whole space.

The MAPW wave functions have the following expression [28]:

$$\psi_{b\boldsymbol{k}}(\boldsymbol{r}) = \sum_{\boldsymbol{K}_j} v(\boldsymbol{k}, \boldsymbol{K}_j) \exp[i(\boldsymbol{k}, \boldsymbol{K}_j)\boldsymbol{r}] + \text{Ⓗ}(r_0 - |\boldsymbol{r}|) \sum_{l=0}^{L} (2l + 1)\, i^l \sum_{v=1}^{2l+1} \eta_{lv} \times \left\{ \sum_n A_{nlv}\, R_{nl}(r) - \sum_{\boldsymbol{K}_j} v(\boldsymbol{k}, \boldsymbol{K}_j)\, y_{lv} \times [(\boldsymbol{k} + \boldsymbol{K}_j)^0]\, j_l(|\boldsymbol{k} + \boldsymbol{K}_j|\, r) \right\} y_{lv}(\boldsymbol{r}^0) \quad \text{(A5)}$$

where: $\boldsymbol{K}_j$ = a reciprocal lattice vector, b = band index, Ⓗ(x) = Heaviside step function,

$$\text{Ⓗ}(x) = \begin{cases} 0 & x < 0 \\ 1 & x > 0 \end{cases}$$

$j_l(x)$ = spherical Bessel function, R_{nl} = the solution of the radial differential equation, L = the maximum angular momentum quantum number, which is taken equal to 2, i.e. $l = 0, 1, 2$, throughout this paper and n = the number of zeros of R_{nl} at the interval $0 < r \leqslant r_0$.

The real valued spherical harmonic functions y_{lv} are defined as:

$$y_{lv}(\theta, \phi) = \begin{cases} (l - m)!/l!\, P_l^m(\cos\theta) \cos m\phi & \begin{matrix} v = 2m + 1 \\ m = 0, \ldots l \end{matrix} \\ (l - m)!/l!\, P_l^m(\cos\theta) \sin m\phi & \begin{matrix} v = 2m \\ m = 1, \ldots l \end{matrix} \end{cases} \quad \text{(A6)}$$

They have the following orthogonality relations:

$$\int_\Omega y_{lv}(\boldsymbol{r}^0)\, y_{l'v'}(\boldsymbol{r}^0)\, \mathrm{d}\Omega = \frac{4\pi}{2l + 1} \frac{1}{\eta_{lv}} \delta_{ll'}\, \delta_{vv'}$$

with

$$\eta_{lv} = \begin{cases} 1 & \text{for } v = 1 \\ \dfrac{2(l!)^2}{(l - m)!(l + m)!} & \text{for } v > 1 \end{cases} \quad \text{(A7)}$$

The coefficients A_{nlv} and $v(\boldsymbol{k}, \boldsymbol{K}_j)$ satisfy the continuity conditions [29]

$$\sum_{\boldsymbol{K}_j} v(\boldsymbol{k}, \boldsymbol{K}_j)\, y_{qv}[(\boldsymbol{k} + \boldsymbol{K}_j)^0]\, j_l(|\boldsymbol{k} + \boldsymbol{K}_j| r_0) = \sum_n A_{nlv}\, R_{nl}(r_0),$$

$$\sum_{\boldsymbol{K}_j} v(\boldsymbol{k}, \boldsymbol{K}_j)\, y_{lv}[(\boldsymbol{k} + \boldsymbol{K}_j)^0] \frac{\mathrm{d}}{\mathrm{d}r} j_l(|\boldsymbol{k} + \boldsymbol{K}_j| r)\Big|_{r_0} = \sum_n A_{nlv} \frac{\mathrm{d}}{\mathrm{d}r} R_{nl}(r)\Big|_{r_0} \quad \text{(A8)}$$

which guarantee the wave functions and their first derivatives to be continuous across the surface of the APW spheres.

Appendix 3. The matrix elements $\langle \boldsymbol{b'}, \boldsymbol{k} + \boldsymbol{q} + \boldsymbol{Q}^* \mid \exp(i\boldsymbol{qr}) \mid \boldsymbol{b}, \boldsymbol{k} \rangle$

We give here the expression of these matrix elements in the MAPW method [6]

$$\langle b, \boldsymbol{k} + \boldsymbol{q} + \boldsymbol{Q}^* \mid \exp(i\boldsymbol{qr}) \mid b\boldsymbol{k} \rangle = \sum_{j',j} v^*(\boldsymbol{k} + \boldsymbol{q} + \boldsymbol{Q}^*, \boldsymbol{K}_{j'})\, v(\boldsymbol{k}, \boldsymbol{K}_j)\, S_{j',j} + \sum_{j',nlv} v^*(\boldsymbol{k} + \boldsymbol{q} + \boldsymbol{Q}^*, \boldsymbol{K}_{j'})\, A_{nlv} S_{j',nlv} + \sum_{n'l'v',j} A^*_{n'l'v'}\, v(\boldsymbol{k}, \boldsymbol{K}_j)\, S_{n'l'v',j} + \sum_{n'l'v'nlv} A^*_{n'l'v'}\, A_{nlv}\, S_{n'l'v',nlv} \quad \text{(A9)}$$

To simplify the equations, let us use the following

abbreviations:

$$\mathrm{SCG}(lv, l'v', l''v'') = \frac{1}{4\pi} i^{l-l'+l''} \times (2l+1)(2l'+1)(2l''+1)\,\eta_{lv}\,\eta_{l'v'}\,\eta_{l''v''} \times \int_\Omega y_{lv}(\boldsymbol{r}^0)\, y_{l'v'}(\boldsymbol{r}^0)\, y_{l''v''}(\boldsymbol{r}^0)\,\mathrm{d}\Omega$$

$$\frac{4\pi}{v_c}\int_0^{r_0} j_l(\alpha r)\, j_{l'}(\beta r)\, j_{l''}(\gamma_r)\, r^2\,\mathrm{d}r := JJJ_{l,l',l''}(\alpha,\beta,\gamma)$$

v_c is the volume of the primitive unit cell

$$\frac{4\pi}{v_c}\int_0^{r_0} j_l(\alpha r)\, j_l(\beta r)\, r^2\,\mathrm{d}r := JJ_l(\alpha,\beta)$$

$$\frac{4\pi}{v_c}\int_0^{r_0} R_{nl}(r)\, j_l(|\boldsymbol{p}|\, r)\, r^2\,\mathrm{d}r := RJ_l^n(|\boldsymbol{p}|)$$

$$\frac{4\pi}{v_c}\int_0^{r_0} R_{nl}(r)\, j_{l'}(|\boldsymbol{p}|\, r) j_{l''}(|\boldsymbol{q}|\, r) r^2\,\mathrm{d}r := RJJ^n_{l,l',l''}(|\boldsymbol{p}|,|\boldsymbol{q}|)$$

and

$$\frac{4\pi}{v_c}\int_0^{r_0} R_{nl}(r)\, R_{n'l'}(r)\, j_{l''}(|\boldsymbol{q}|\, r)\, r^2\,\mathrm{d}r := RRJ^{n,n'}_{l,l',l''}(|\boldsymbol{q}|) \tag{A10}$$

It is to be noticed that $(l - l' + l'')$ in the Glebsch–Gordan coefficients, SCG, is an even number, i.e. those coefficients are real.

With definitions (A10) the submatrices, S, have the form:

$$\begin{aligned} S_{j'j} &= \delta_{\boldsymbol{K}_j - \boldsymbol{K}_{j'} - \boldsymbol{Q}^*} - \sum_{l=0}^{L}\sum_{v=1}^{2l+1}(2l+1)\eta_{lv}\, y_{lv}(\boldsymbol{k}+\boldsymbol{K}_j) \\ &\times y_{lv}(\boldsymbol{k}+\boldsymbol{Q}^*+\boldsymbol{K}_{j'}) \\ &\times JJ_l(|\boldsymbol{k}+\boldsymbol{K}_j|, |\boldsymbol{k}+\boldsymbol{K}_j+\boldsymbol{Q}^*|) \\ &- \sum_{l=0}^{L}\sum_{v=1}^{2l+1}(2l+1)\,\eta_{lv} y_{lv} \\ &\times (\boldsymbol{k}+\boldsymbol{q}+\boldsymbol{Q}^*+\boldsymbol{K}_{j'})\, y_{lv}(\boldsymbol{k}+\boldsymbol{q}+\boldsymbol{K}_j) \\ &\times JJ_l(|\boldsymbol{k}+\boldsymbol{K}_j+\boldsymbol{q}|, |\boldsymbol{k}+\boldsymbol{q}+\boldsymbol{Q}^*+\boldsymbol{K}_{j'}|) \\ &+ \sum_{l,l'}\sum_{l''=|l-l'|}^{l+l'}\sum_{v,v',v''}\mathrm{SCG}(lv, l'v', l''v'') \\ &\times y_{lv}(\boldsymbol{k}+\boldsymbol{K}_j)\, y_{l''v''}(\boldsymbol{q})\, y_{l'v'}(\boldsymbol{k}+\boldsymbol{q}+\boldsymbol{Q}^*+\boldsymbol{K}_j) \\ &\times JJJ_{(l,l',l'')}(|\boldsymbol{k}+\boldsymbol{K}_j|, \\ &\times |\boldsymbol{k}+\boldsymbol{q}+\boldsymbol{Q}^*+\boldsymbol{K}_j|, |\boldsymbol{q}|), \end{aligned} \tag{A11}$$

$$\begin{aligned} S_{j',nlv} &= (2l+1)\,\eta_{lv}\, RJ_l^n(|\boldsymbol{k}+\boldsymbol{Q}^*+\boldsymbol{K}_{j'}|) \\ &\times y_{lv}(\boldsymbol{k}+\boldsymbol{Q}^*+\boldsymbol{K}_{j'}) \\ &- \sum_{l',l'',v',v''}\mathrm{SCG}(lv, l'v', l''v'')\, y_{l''v''}(\boldsymbol{q})\, y_{l'v'} \\ &\times (\boldsymbol{k}+\boldsymbol{q}+\boldsymbol{Q}^*+\boldsymbol{K}_{j'})\, RJJ^n_{l,l'l''} \\ &\times (|\boldsymbol{k}+\boldsymbol{q}+\boldsymbol{Q}^*+\boldsymbol{K}_{j'}|, |\boldsymbol{q}|) \end{aligned} \tag{A12}$$

$$\begin{aligned} S_{n'l'v',j} &= (2l'+1)\,\eta_{l'v'}\, RJ_{l'}^{n'}(|\boldsymbol{k}+\boldsymbol{q}+\boldsymbol{K}_j|) \\ &\times y_{l'v'}(\boldsymbol{k}+\boldsymbol{q}+\boldsymbol{K}_j) \\ &- \sum_{l,l'',v,v''}\mathrm{SCG}(lv, l'v', l''v'') \\ &\times y_{l''v''}(\boldsymbol{q})\, y_{lv}(\boldsymbol{k}+\boldsymbol{K}_j) \\ &\times RJJ^{n'}_{l',l,l''}(|\boldsymbol{k}+\boldsymbol{K}_j|, |\boldsymbol{q}|) \end{aligned} \tag{A13}$$

and $S_{n'l'v',nlv}$ is given by:

$$\begin{aligned} S_{n'l'v',nlv} &= \sum_{l'',v''}\mathrm{SCG}(lv, l'v', l''v'')\, y_{l''v''}(\boldsymbol{q}) \\ &\times RRJ^{n,n'}_{l,l',l''}(|\boldsymbol{q}|) \end{aligned} \tag{A14}$$

For the evaluations of these integrals, the programs used and the fine details of the calculations, see [4].

Appendix 4. The Lindhard function

The real part of the Lindhard dielectric function, $\varepsilon_1^{\mathrm{Lind}}(|\boldsymbol{q}|, \omega)$ can be written as [26]

$$\varepsilon_1^{\mathrm{Lind}}(|\boldsymbol{q}|, \omega)\; 1 + \frac{e^2}{2\pi k_f}\frac{1}{\alpha^3} \times \left[\phi\left(\alpha + \frac{\beta}{\alpha}\right) + \phi\left(\alpha - \frac{\beta}{\alpha}\right)\right] \tag{A15}$$

where

$$\alpha = |\boldsymbol{q}|/k_f, \quad \beta = \hbar\omega/k_f^2$$

and k_f is the radius of the Fermi sphere, with

$$\phi(\gamma) = \gamma + \left(1 - \frac{\gamma^2}{4}\right)\ln\left|\frac{\gamma+2}{\gamma-2}\right| \tag{A16}$$

For all non-zero values of $|\boldsymbol{q}|$, the $\varepsilon_1^{\mathrm{Lind}}(|\boldsymbol{q}|, \omega)$ decreases with increasing ω, so that the maximum value of $\varepsilon_1^{\mathrm{Lind}}$ always occurs at $\omega = 0$ and then decreases to a minimum negative value and then increases to a constant value, which is slightly less than one.

As $|\boldsymbol{q}|$ becomes greater than 0.703 $(2\pi/a)$, $\varepsilon_1^{\mathrm{Lind}}(|\boldsymbol{q}|, \omega)$ is always positive for all frequencies. Its value decreases with ω and reaches its minimum positive value at $\omega_{\min}$ then increases to a constant value, which is slightly greater than one.

In the present range of energy, $2 < \hbar\omega \leqslant 4\,\mathrm{Ry}$, $\varepsilon_1^{\mathrm{Lind}}(|\boldsymbol{q}|, \omega)$ is positive for all wave vectors, which is the same behaviour as in all real metals.

For the sake of comparison and the completeness of the Lindhard function for homogeneous electron gas, we give the analytical form of $\varepsilon_2^{\mathrm{Lind}}(|\boldsymbol{q}|, \omega)$

$$\varepsilon_2^{\mathrm{Lind}}(|\boldsymbol{q}|, \omega) = \frac{e^2}{2k_f}\frac{1}{\alpha^3}\left[\chi\left(\alpha + \frac{\beta}{\alpha}\right) - \chi\left(\alpha - \frac{\beta}{\alpha}\right)\right] \tag{A17}$$

where

$$\chi(\gamma) = \left(1 - \frac{\gamma^2}{4}\right)[\text{Ⓗ}(\gamma+2) - \text{Ⓗ}(\gamma-2)] \tag{A18}$$

with

$$\text{Ⓗ}(\delta) = \begin{cases} 1 & \delta > 0 \\ 0 & \delta < 0 \end{cases}$$

It is easy to notice from Equation A17 that $\varepsilon_2^{\mathrm{Lind}}(|\boldsymbol{q}|, \omega)$ at first increases linearly and then falls quadratically with ω for each $|\boldsymbol{q}|$. Also that $\varepsilon_2^{\mathrm{Lind}}(|\boldsymbol{q}|, \omega = 0)$ is equal to zero, which is the same behaviour as in real metals.

References

1. P. NOZIÉRES and D. PINES, *Phys. Rev.* **1** (1959) 1254.
2. H. RAETHER, "Springer Tracts in Modern Physics",

Vol. 38 (Springer, Berlin, 1965) p. 85.
3. J. DANIELS, D. FESTENBERG, H. RAETHER and K. ZEPPENFIELD, *ibid.* Vol. 54 (1970) p. 77.
4. A. SEOUD, Dissertation, Faculty of Physics, Ludwig-Maximilians University, Munich (1983), unpublished.
5. A. SEOUD, *Arabian J. Sci. Engng* **13** (1988) 87.
6. *Idem, ibid.* **13** (1988) in press.
7. S. ADLER, *Phys. Rev.* **126** (1962) 413.
8. M. CHODOROW, PhD thesis, Massachusetts Institute of Technology (1939), unpublished.
9. G. BURDICK, *Phys. Rev.* **129** (1963) 138.
10. D. CHADI and M. COHEN, *ibid.* **B8** (1973) 5747.
11. H. MONKHORST and J. PACK, *ibid.* **B13** (1976) 5188.
12. Y. KUBO, *J. Phys. Soc. Jpn* **40** (1976) 1339.
13. B. MEKKI, personal communications (1983).
14. *Idem,* Dissertation, Faculty of Physics, Ludwig-Maximilians University, Munich (1986).
15. H. HAGEMANN, W. GUDAT and C. KUNZ, *J. Opt. Soc. Amer.* **65** (1975) 742.
16. Y. KUBO, S. WAKOH and J. YAMASHITA, *J. Phys. Soc. Jpn* **41** (1976) 1556.
17. C. KITTEL, "Introduction to Solid State Physics", 5th Edn (Wiley Eastern, New Delhi, 1984) p. 323.
18. C. WEHENKEL, *J. de Physique* **36** (1975) 199.
19. L. FELDKAMP, L. DAVIS and M. STEARNS, *Phys. Rev.* **B15** (1977) 5535.
20. M. CREUZBURG, *Z. Phys.* **196** (1966) 433.
21. C. WEHENKEL and GAUTHÉ, *Solid State Commun.* **15** (1974) 555.
22. R. HAENSEL, C. KUNZ and B. SONNTAG, *Phys. Lett.* **25A** (1967) 205.
23. C. WEHENKEL and B. GAUTHÉ, *Opt. Commun.* **11** (1974) 62.
24. R. HAENSEL, C. KUNZ, T. SASAKI and B. SONNTAG, *DESY* **67/27** (August 1967).
25. B. SONNTAG, R. HAENSEL and C. KUNZ, *DESY* **69/6** (January 1969).
26. J. LINDHARD, *Kgl. Danske Videnskab. Selskab, Mat.-Fys. Medd.* **28** (1954) 8.
27. R. LÄSSER, N. SMITH and R. BENBOW, *Phys. Rev. B* **24** (1981) 1895.
28. H. BROSS, *Phys. Kond. Mater.* **3** (1964) 119.
29. *Idem, Z. Phys.* **215** (1968) 485.

The reader is also referred to:

30. O. BELHACHENI, "Berechnung der Transversalen Mikroskopischen Dielectrischen Funktion von Kupfer", Dissertation, Faculty of Physics, Ludwig-Maximilians University, Munich (1986).
31. F. WOOTEN, "Optical Properties of Solids" (Academic, New York, 1972).

Received 25 March
and accepted 22 September 1987